



This article appeared in a journal published by Elsevier. The attached copy is furnished to the author for internal non-commercial research and education use, including for instruction at the authors institution and sharing with colleagues.

Other uses, including reproduction and distribution, or selling or licensing copies, or posting to personal, institutional or third party websites are prohibited.

In most cases authors are permitted to post their version of the article (e.g. in Word or Tex form) to their personal website or institutional repository. Authors requiring further information regarding Elsevier's archiving and manuscript policies are encouraged to visit:

<http://www.elsevier.com/copyright>



Contents lists available at ScienceDirect

Journal of the Mechanics and Physics of Solids

journal homepage: www.elsevier.com/locate/jmps

Dynamics of structural interfaces: Filtering and focussing effects for elastic waves

M. Brun^{a,1}, S. Guenneau^b, A.B. Movchan^b, D. Bigoni^{c,*}

^a Department of Structural Engineering, University of Cagliari and Istituto CNR-IOM, Unità SLACS, Piazza d'Armi, I-09123 Cagliari, Italy

^b Department of Mathematical Sciences, University of Liverpool, Liverpool L69 3BX, UK

^c Department of Mechanical and Structural Engineering, University of Trento, Via Mesiano 77, I-38050 Trento, Italy

ARTICLE INFO

Article history:

Received 3 November 2009

Received in revised form

27 May 2010

Accepted 19 June 2010

Keywords:

Elastic waves

Structural interfaces

Transfer matrix

Filtering by finite thickness slabs

Negative refraction

ABSTRACT

Dynamics of thick interfaces separating different regions of elastic materials is investigated. The interfaces are made up of elastic layers or inertial truss structures. The study of evanescent mode propagation and transmission properties reveals that the discrete nature of structural interfaces introduces unusual filtering characteristics in the system, which cannot be obtained with multilayered interfaces. An example of metamaterial is presented, namely, a planar structural interface, which acts as a flat lens, therefore evidencing the negative refraction and focussing of elastic waves.

© 2010 Elsevier Ltd. All rights reserved.

1. Introduction

The concept of *structural interface* has been introduced by Bigoni and Movchan (2002) to model a situation broadly encountered in natural and artificial systems, where a real structure—possessing finite-thickness—joins continuous materials. In elastostatics, Bertoldi et al. (2007a, b) have shown that the introduction of structural interfaces involves a non-local mechanical behaviour and allows the achievement of special mechanical properties (such as mending of elastic stress concentrations), particularly in composite materials and in the related problem of bridged cracks (Bertoldi et al., 2007c). Independent results supporting the findings by Bertoldi et al. have been presented by Tang et al. (2005), with reference to the problem of adhesion, and by Sumigawa et al. (2008), who provide experimental observation of imperfect interfaces consisting of nano-springs (Robbie et al., 1996, 1999).

Bigoni and Movchan (2002) noticed that a *thick interface*² possesses a mass that can strongly influence dynamic characteristics, both for structural interfaces and for interfaces made up of inertial elastic layers. In this field, their preliminary calculations performed for Bloch–Floquet waves in stratified structured media demonstrate that structural

* Corresponding author. Tel.: +39 0461 882507; fax: +39 0461 882599.

E-mail addresses: mbrun@unica.it (M. Brun), guenneau@liverpool.ac.uk (S. Guenneau), abm@liv.ac.uk (A.B. Movchan), bigoni@ing.unitn.it (D. Bigoni).

URLS: <http://people.unica.it/brunmi/> (M. Brun), <http://www.maths.liv.ac.uk/~guenneau/> (S. Guenneau), <http://www.maths.liv.ac.uk/~abm/>

(A.B. Movchan), <http://www.ing.unitn.it/~bigoni/> (D. Bigoni).

¹ Tel.: +39 070 6755411; fax: +39 070 6755418.

² The adjective 'thick' is used here to contrast with the known models of zero-thickness interfaces, see for a description Bertoldi et al. (2007a). Zero-thickness interfaces have been tailored to provide a relation between traction and jump in displacement, without consideration of inertial effects.

interfaces can be designed to determine unusual filtering properties for elastic waves.³ Similar calculations on periodic structures and composites have been performed by various authors,⁴ however they all address *periodic* structures, while a structural interface commonly occurs ‘isolated’, say, in a non-periodic manner. Therefore, an aim of the present article is to characterize dynamic response of non-periodic structural interfaces, made up of a finite-thickness stack of elastic layers, or combinations of elastic layers alternated with truss-like structures (so that we assign the name ‘structural interface’ to all interfaces in which a discrete structure is present). Filtering properties of these structures are compared, giving evidence of behaviours typical of discreteness, via the transfer matrix techniques (used to analyze interaction of electromagnetic waves with stratified structures by Lekner, 1994 and Felbacq et al., 1998), which enable us to characterize localization, filtering and polarization properties of the given discrete-continuous systems within a given frequency range. In particular, the following results are found.

- Structural interfaces are shown to provide filtering properties which remain unchallenged employing layered interfaces. It is shown for instance that a structural interface can be designed to filter an extremely narrow range of frequencies, while infinite frequencies are always transmitted employing layered interfaces. Moreover, a class of slow waves propagating within structural and layered interfaces with a low reflection coefficient is identified. Although in the low frequency limit the reflection properties of both interfaces are similar, a visible difference is found in reflection of slow waves for frequencies corresponding to the optical bands in the dispersion diagrams.
- Simple models for the analysis of propagation of evanescent waves within structural and layered interfaces are provided, so that the frequencies can be found corresponding to the maximum exponential decay, in other words, to the maximum wave attenuation. These simple models represent the necessary tool for the design of optimal insulating devices.
- Periodic systems are known to support waves of low group velocities, so that they can be used as delay line devices. However, the reflection of the elastic energy at a thick interface is an important issue limiting the performance of these devices. Simple models are shown to provide the way to tune the reflection and transmission coefficients of these systems within a given frequency range.

In parallel with the above-mentioned studies, topical research has grown upon the so-called ‘metamaterials’, which for electromagnetic waves are composite nanomaterials structured on a scale smaller than the wavelength (Pendry et al., 1999) and for elastic waves are material exhibiting exponential localization of vibration modes for a certain frequency range (Movchan and Guenneau, 2004; Movchan and Slepyan, 2007; Guenneau et al., 2007) and displaying ‘negative mass density effects’ (Milton and Willis, 2007).

Metamaterials can also be tailored to produce the so-called ‘wave cloaking’, namely, a system guiding waves around an object to make it ‘invisible’ (Pendry et al., 2006; Leonhardt and Philbin, 2006) or a negatively refracting shell displaying anomalous resonances hiding a set of dipole sources located nearby (Milton and Nicorovici, 2006; Milton et al., 2008). In particular, the first experimental observation of acoustic cloaking was reported by Farhat et al. (2008) for linear surface waves in a fluid, while a numerical proof of cloaking of coupled in-plane pressure and shear waves was reported by Brun et al. (2009).

An aim of the present article is to show that *structural interfaces can be designed to produce metamaterials for elastic waves*, so that the two concepts are bridged. Therefore, as electromagnetic metamaterials were experimentally shown to lead to a negative index of refraction (Smith and Kroll, 2000),⁵ and to focus acoustic signals through structured slab lens (Guenneau et al., 2007; Ding et al., 2007; Sukhovich et al., 2008; Zhang et al., 2009), *we extend these results to elastic waves, providing an example of a structural interface that can exhibit negative refraction and produce imaging of a vibrating source*. This result leads to a possible design of a flat interface, evidencing focussing of elastic signal of a desired frequency.

The structure of the present article is as follows. Geometry of a structural interface and a certain class of asymptotic approximations are given in Section 2. The transfer matrix method is applied in Section 3 to investigate the dispersion, filtering and transmission properties of structural and layered interfaces of finite width. Finally, focussing of the elastic signal via interaction with a structural interface and the effects of negative refraction are addressed in Section 4.

³ Parnell (2007), Bigoni et al. (2008) and Gei et al. (2009) have shown that dynamical properties can be strongly influenced by prestress, which may be used as a tuning parameter in the design of filtering devices for elastic waves.

⁴ Elastic Bloch–Floquet waves in inhomogeneous lattice structures were studied by Martinsson and Movchan (2003), addressing band gap properties for both truss and frame like structures. Spectral properties of elastic waves in a doubly periodic array of coated inclusions were analyzed by Platts and Movchan (2004). In particular, for the case of soft anisotropic coating, the effective conditions of imperfect interface were imposed on the inclusion boundaries, and it has been shown that the stiffness parameters of such a coating can be chosen in such a way that the inclusions become neutral in the long-wave limit. The influence of perturbation of the geometry for periodic stacks on the band gap structure was analyzed by Guenneau et al. (2008).

⁵ Negative index refraction makes a focussing flat lens possible, as theorized by Veselago (1968) and further can lead to sub-wavelength imaging (Pendry, 2000).

2. Structural interface and the corresponding homogenization approximation

We begin with the description of the structural interface, which is used to filter or slow down elastic waves within certain frequency intervals. In particular, we follow Bigoni and Movchan (2002), where inertial interfaces have been introduced in the model of coated inclusions and the corresponding dynamic properties have been linked to the theory of Bloch–Floquet waves in structured media.

We select the geometry of the structural interface as shown in Fig. 1. In the figure, the basic unit cell (of thickness d) is shown on the right and is made up of two elastic layers of thickness $d_0/2$ (mass density ρ_0 and shear modulus μ_0) and two massless truss-structures connected through a stiff layer (sketched black), which ‘condenses’ the mass m of the structure. The structural interface joins two isotropic elastic media (of mass density ρ_α and ρ_β and shear stiffness μ_α and μ_β) and is made up of a p -times repetition of the unit cell ($p \in \mathbb{N}^+ \setminus \{0\}$), so that the interface has a thickness pd .

We note the following two special cases: (i) the interface is reduced to an inertial truss structure made up of two massless truss structures containing a ‘heavy’ layer and dividing an elastic space, when $p=1$ and the elastic layers of the unit cell are identical to the elastic media jointed by the interface; (ii) a periodic structure alternating elastic layers with inertial truss-structures is obtained when $p \rightarrow \infty$.

Direct analytical treatment of the interfacial structure shown in Fig. 1 is awkward due to structural complexity, but can be pursued numerically (and such calculations will in particular be used to obtain results on negative refraction presented in Section 4). In addition to the numerical approach, we feel crucial for design purposes to provide simple analytical approximations of the interface, useful in the characterization of the dynamical properties of the structure in a wide range of the frequency spectrum. The simplest approximation of the unit cell shown in Fig. 1 on the right is the interface shown in Fig. 2a consisting of a two-layer continuous elastic system and labeled ‘layered interface’ in the following. This can be conveniently employed in the case of shear plane waves polarized parallel to the interface, that will be addressed in Section 3.

For more general purposes, the simplified unit cell shown in Fig. 2b can be employed and this will be addressed as ‘structural interface’. When compared to the layered model, the structural system evidences special properties, that will be addressed later.

In order to represent an approximation of the unit cell shown in Fig. 1 on the right, the stiffness of the system has to be calibrated. In particular, as indicated in Fig. 1 on the right, the elementary cell of the structure, periodic in the vertical direction, includes thin elastic bars inclined at a certain angle η . Following the scheme of Fig. 2b, the simplified structure is reduced to a longitudinal spring of effective stiffness

$$\gamma = \frac{EA}{d_1^2} \sin\eta \cos^2 \eta + \hat{\gamma}, \tag{1}$$

where E is the Young modulus and A the area per unit thickness of the bars forming the truss structure and $\hat{\gamma}$ is a correction factor introduced to take into account the flexural behaviour of the bars. We also have an inertial, stiff layer within the

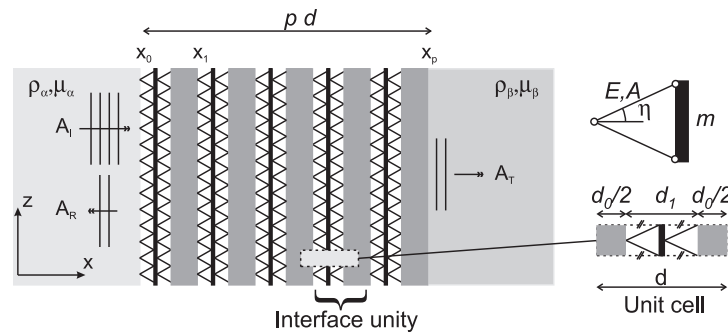


Fig. 1. Layered structural interface of thickness pd joining two elastic media with shear modulus μ_j and density ρ_j ($j = \alpha, \beta$). The interface is obtained as a p -times repetition of the unit cell shown on the right.

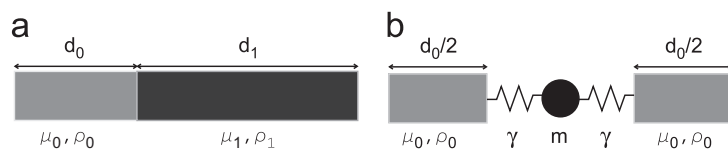


Fig. 2. Approximations to the interface unit cell shown in Fig. 1 on the right. (a) Bilayered unit cell: the continuous phases have shear moduli μ_0 and μ_1 , densities ρ_0 and ρ_1 and thicknesses d_0 and d_1 , respectively. (b) Structural unit cell: the continuous phase has shear modulus μ_0 , density ρ_0 and total thickness d_0 , the spring–mass system has stiffness γ and mass m .

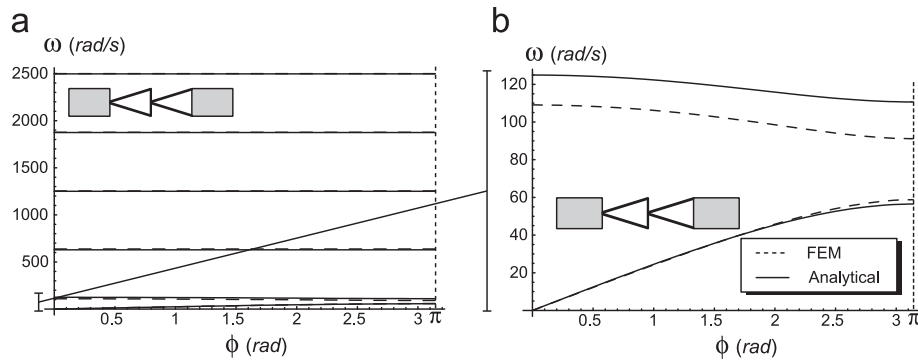


Fig. 3. Dispersion diagram for a truss-like structural interface compared to the spring/mass model. (a) Initial six frequency pass bands. (b) Detail of (a): the acoustical branch and the first optical branch. Analytical solution is given in solid lines, numerical simulations in dashed lines.

structural interface, which is ‘condensed’ in the concentrated mass m shown in Fig. 2b. Since the layer is assumed rigid when compared to the stiffness of the truss-like structure, it does not affect Eq. (1), at least in a first approximation.

To prove the consistency of the approximation (1), we consider the structure shown in Fig. 1, made periodic taking the number of unit cells $p \rightarrow \infty$. Anticipating results obtained in Section 3.2, we show here that the in-plane elastic Bloch–Floquet waves (Eq. (17)) propagating orthogonally and polarized parallel to the interfaces (i.e. in antiplane shearing—Eq. (2)) through the infinite structure have dispersion properties similar to those found in the simpler structure obtained adopting the unit cell shown in Fig. 2b, with the choice (1) and $\hat{\gamma} = 0$ of the homogenization parameters. In particular, the dispersion equation (15) for the structure reported in Fig. 2b can be obtained in a closed analytical form and then solved numerically with respect to the circular frequency ω for fixed values of the Bloch parameter ϕ . Results are reported in Fig. 3 and compared with a finite element calculation of the whole structure.⁶

It is noted that the acoustic branches reported in Figs. 3a and b (the latter is a detail of the former) for the structural interface and its ‘spring/mass’ approximation are almost identical, whereas a small discrepancy is observed only in the first optical branch. For higher frequencies there is an optimal agreement between finite-element and analytical results up to the point in which the eigenmodes of the low density inclined bars are excited by the wave propagation.

This illustrative computation suggests that the simple geometry of Fig. 2b can be used to approximate low frequency wave propagation within solids containing the structural interface shown in Fig. 1.

In the sequel of this paper, we shall use the *transfer matrix method* to analyze not only infinite structures, but also finite thickness interfaces, which can be designed to slow down waves of certain frequency and polarization.

3. Filtering by layered metamaterials

In order to design a structural interface to possess desired filtering properties, analytical formulae become of primary importance, so that we approximate the structural interface shown in Fig. 1 replacing the unit cell shown on the right with the structural unit cell shown in Fig. 2b and with the layered cell shown in Fig. 2a.

Instead of limiting our study only to Bloch–Floquet waves, we address the problem using the transfer matrix method, which has been developed in the recent literature and extended to the related homogenization problems (see Lekner, 1994; Felbacq et al., 1998). A brief outline of the method is given below, with emphasis on the contribution of the discrete part of the structure. Finally, we draw a comparison between the transmission properties of structural (Fig. 2b) and layered (Fig. 2a) interfaces, showing that unusual properties, such as negative refraction, can be attributed to the structural model. This leads to the construction of flat lens devices, which may refocus elastic waves generated by a finite size source on the other side of the structural slab, a problem attacked in Section 4 with a numerical technique directly on the structure shown in Fig. 1 and showing the reason to refer to materials of such type as ‘metamaterials’.

⁶ A finite element model (built in Comsol® ver. 3.5) has been used to simulate the Bloch–Floquet waves propagating within the two-dimensional structure of Fig. 1. For the case when the wave vector is aligned with the x -axis we construct the dispersion diagram, which shows the frequency ω as a function of the Bloch parameter ϕ (see Fig. 3). The parameters used for this computation are as follows:

- elastic continua joined by the interface: $E=200$ MPa, $\nu = 0.3$, $\rho = 7800$ kg/m³,
- bars of the truss structures: $E=10$ MPa, $\nu = 0.3$, $\rho = 10$ kg/m³, $A=0.1$ m²/m, $\eta = 0.2$ rad,
- inertial layers: $E=2 \times 10^6$ MPa, $\nu = 0.3$, $\rho = 452.273.9$ kg/m³.

3.1. Transfer matrix method for structural interfaces

Let us consider the layered structure reported in Fig. 1 with the unit cells shown in Fig. 2. For simplicity, we restrict the analysis to antiplane harmonic shear waves propagating at normal incidence and we indicate with $u(x)$ the component of the displacement along the z -axis.

3.1.1. Elastic layer

The field equation of time-harmonic motion with circular frequency ω for an elastic layer of thickness d , characterized by a shear modulus μ and density ρ is given by

$$\frac{\partial^2 u(x)}{\partial x^2} + \frac{\rho}{\mu} \omega^2 u(x) = 0. \quad (2)$$

The wave form can be expressed in terms of complex amplitudes A and B as

$$u(x) = A \exp(ikx) + B \exp(-ikx), \quad (3)$$

where i is the imaginary unit and the wave number k is related to the circular frequency by

$$k = \omega c, \quad c = \sqrt{\frac{\rho}{\mu}}, \quad (4)$$

so that $c\mu = \sqrt{\rho\mu}$ is the *elastic impedance* and the equation of motion (2) results to be now automatically satisfied.

At the layer interfaces, located at $x=x_0$ and $x=x_1=x_0+d$, displacements and tractions are related through the *transfer matrix* $[\mathbf{M}] = m_{ij}$, defined as

$$\begin{bmatrix} u(x_1) \\ \mu \frac{\partial u}{\partial x}(x_1) \end{bmatrix} = \begin{bmatrix} m_{11} & m_{12} \\ m_{21} & m_{22} \end{bmatrix} \begin{bmatrix} u(x_0) \\ \mu \frac{\partial u}{\partial x}(x_0) \end{bmatrix}. \quad (5)$$

Using the expression (3) we can obtain the transfer matrix in the form

$$\mathbf{M} = \begin{bmatrix} \cos \delta & \frac{\sin \delta}{Q} \\ -Q \sin \delta & \cos \delta \end{bmatrix}, \quad (6)$$

where $Q = \mu k$ and $\delta = kd$ is the *phase increment*.

Note that the eigenvalues of the transfer matrix (6) are

$$\cos \delta \pm \sqrt{\cos^2 \delta - 1} = \exp(\pm i\delta). \quad (7)$$

3.1.2. Structural interface

We consider now a structural interface as depicted in Fig. 2b where the structural part is made up of two springs and a concentrated mass. Now, the transfer matrix is defined to connect the displacements and forces (per unit length) on the right to the same functions evaluated on the left, and calculations on the structural part invoking time-harmonic behaviour allow us to obtain the matrix

$$\mathbf{M} = \begin{bmatrix} \frac{\gamma - m\omega^2}{\gamma} & \frac{2\gamma - m\omega^2}{\gamma^2} \\ -m\omega^2 & \frac{\gamma - m\omega^2}{\gamma} \end{bmatrix}, \quad (8)$$

which is unimodular.

The eigenvalues of the transfer matrix (8) are

$$1 - \frac{m}{\gamma} \omega^2 \pm \sqrt{\frac{m}{\gamma} \omega^2 \left(\frac{m}{\gamma} \omega^2 - 2 \right)}, \quad (9)$$

so that the dependence on the circular frequency ω is algebraic for the structural interface, while it is trigonometric for a continuous layer, as shown by Eq. (7). Moreover, the eigenvalues (9) are necessarily complex (real) at sufficiently small (high) frequency.

3.1.3. Two-element systems

For the systems shown in Fig. 2 the transfer matrix is obtained through multiplication of the matrices corresponding to the single elements. In particular, for the bilayer shown in Fig. 2a, we have to multiply two matrices of the type (6),

thus obtaining

$$\mathbf{M} = \begin{bmatrix} \cos\delta_0\cos\delta_1 - \frac{Q_0}{Q_1}\sin\delta_0\sin\delta_1 & \frac{1}{Q_0}\sin\delta_0\cos\delta_1 + \frac{1}{Q_1}\cos\delta_0\sin\delta_1 \\ -Q_0\sin\delta_0\cos\delta_1 - Q_1\cos\delta_0\sin\delta_1 & \cos\delta_0\cos\delta_1 - \frac{Q_1}{Q_0}\sin\delta_0\sin\delta_1 \end{bmatrix}, \quad (10)$$

where δ_i ($i=0,1$) is the phase increment of the i -th phase, and $Q_i = \mu_i k_i$ ($i=0,1$).

For a structural interface made up of an elastic layer connected to a spring/mass/spring system (Fig. 2b), the *structural interface transfer matrix* has the following entries:

$$\begin{aligned} m_{11} &= \frac{\gamma - m\omega^2}{\gamma} \cos\delta_0 - \frac{Q_0(2\gamma - m\omega^2)}{\gamma^2} \sin\delta_0, \\ m_{12} &= \frac{2\gamma - m\omega^2}{\gamma^2} \cos\delta_0 + \frac{\gamma - m\omega^2}{\gamma Q_0} \sin\delta_0, \\ m_{21} &= -m\omega^2 \cos\delta_0 + \frac{Q_0}{\gamma} (m\omega^2 - \gamma) \sin\delta_0, \\ m_{22} &= \frac{\gamma - m\omega^2}{\gamma} \cos\delta_0 - \frac{m\omega^2}{Q_0} \sin\delta_0. \end{aligned} \quad (11)$$

3.1.4. p -Element systems

For a stack of p unit cells of structural (Fig. 2b) or layered (Fig. 2a) type, the transmission and reflection properties can be obtained by simple multiplication of the unimodular unit cell matrix layer defined by Eq. (10) or (11), thus obtaining the transfer matrix

$$\mathbf{M}^p = \begin{pmatrix} m_{11}U_{p-1}(x) - U_{p-2}(x) & m_{12}U_{p-1}(x) \\ m_{21}U_{p-1}(x) & m_{22}U_{p-1}(x) - U_{p-2}(x) \end{pmatrix}, \quad (12)$$

where m_{ij} are the entries of the matrix (10) or (11), $x = (m_{11} + m_{22})/2$ and $U_p(x)$ is the Chebyshev polynomial of the second type⁷ or, equivalently,

$$U_p(\cos\phi) = \begin{cases} \frac{\sin[(p+1)\phi]}{\sin\phi} & \text{for } |x| = |\cos\phi| < 1, \\ (-1)^p \frac{\sinh[(p+1)\xi]}{\sinh\xi} & \text{for } |x| = |\cos\phi| > 1, (\xi = \text{Im}\phi). \end{cases} \quad (13)$$

3.2. Periodic media

We are now in a position to exploit the previous results to solve a periodic infinite medium made up of unit cells consisting of elastic layers alternated with structural interfaces, thus recovering via another route the same results obtained by Bigoni and Movchan (2002).

In particular, considering the two-layer system (10) as the unit cell of an infinite periodic media, we impose that the cell behaves as a single homogeneous elastic layer to obtain the Bloch–Floquet dispersion relation. To achieve this condition, we have to impose coincidence of the eigenvalues of transfer matrices of Eq. (6) (introducing the parameter ϕ instead of δ), and of Eq. (10), which reduces to coincidence of the traces, since the matrices are unimodular. We obtain the condition

$$\cos\phi = \cos(c_0 d_0 \omega) \cos(c_1 d_1 \omega) - \frac{1}{2} \left(\frac{Q_0}{Q_1} + \frac{Q_1}{Q_0} \right) \sin(c_0 d_0 \omega) \sin(c_1 d_1 \omega), \quad (14)$$

which corresponds to the *dispersion relation* obtained by Bigoni and Movchan (2002, their Eq. (38), in which their parameter dh is now ϕ).

In a similar vein, to analyze a periodic structure made up of an elastic layer alternated with a structure, the unit cell shown in Fig. 2b, we impose

$$\cos\phi = \frac{\gamma - m\omega^2}{\gamma} \cos(c_0 d_0 \omega) - \frac{1}{2\gamma} \left[\frac{m\omega^2 \gamma + 2Q_0^2}{Q_0} - Q_0 \frac{m\omega^2}{\gamma} \right] \sin(c_0 d_0 \omega), \quad (15)$$

which corresponds to the *dispersion relation* obtained by Bigoni and Movchan (2002, their Eq. (56), in which their parameter dh is now ϕ).

⁷ $U_0(x)=1$, $U_1(x)=2x$, $U_p(x)=2xU_{p-1}(x) - U_{p-2}(x)$.

In the dispersion equations (14) and (15), ϕ plays the role of the Bloch–Floquet parameter, so that the nature of the solution changes if ϕ has to be taken real or complex. This is ruled by the trace of the transfer matrix \mathbf{M} of the unit cell, connecting displacements and tractions at the left $x=x_N$ and right $x=x_{N+1}$ interfaces of the unit cell as

$$\tilde{\mathbf{u}}_{N+1} = \mathbf{M}\tilde{\mathbf{u}}_N, \quad \tilde{\mathbf{u}}_N = \left[u(x_N), \frac{\partial u}{\partial x}(x_N) \right]^T, \tag{16}$$

so that for the Bloch–Floquet waves

$$\tilde{\mathbf{u}}_{N+1} = \exp(\pm i\phi)\tilde{\mathbf{u}}_N, \quad \phi \in \mathbb{C}, \tag{17}$$

the following different regimes can be classified as follows:

- $|\text{tr}(\mathbf{M})| < 2$: pass band condition, $\tilde{\mathbf{u}}_{N+1} = \exp(\pm i\phi)\tilde{\mathbf{u}}_N$, $\phi \in \mathbb{R}$;
- $\text{tr}(\mathbf{M}) = \pm 2$: standing wave condition, $\tilde{\mathbf{u}}_{N+1} = \pm \tilde{\mathbf{u}}_N$, $\phi = 0, \pi$;
- $|\text{tr}(\mathbf{M})| > 2$: stop band condition, $\tilde{\mathbf{u}}_{N+1} = \pm \exp(-\xi)\tilde{\mathbf{u}}_N$, a solution exponentially decaying, in which $\phi = \pi - i\xi$, or $\phi = i\xi$, $\xi > 0$.

It is important to stress that

$$\xi = \text{Im}(\phi) = \log(|\cos\phi| + \sqrt{\cos^2\phi - 1}), \tag{18}$$

is the analytical expression for the *decay exponent within a given stop band* that has to be maximized to design the maximum attenuation interface (to work within that given stop band).

3.2.1. Comparison between structural interfaces and two-layer systems

The results on periodic systems allow us to quantify effects connected to the presence of structural interfaces within a continuous elastic medium. A comparison between numerical solutions and results provided by Eq. (15) has been anticipated in Fig. 3.

Our interest is now the analysis of more detailed features. In particular, we show that although for propagating modes at low frequencies the homogenization approximation of the structural system leads to a continuum limit described by the layered interface of Fig. 2a, the higher frequency vibrations as well as evanescent modes may differ for the cases of layered and structural systems. This is illustrated below by a comparative analysis of the dispersion diagrams.

In Fig. 4 the *dispersion curves* are plotted for layered and structural interfaces. Results for bilayered interfaces are shown in Fig. 4a with

$$\mu_0 = 76.9 \text{ MPa}, \quad \rho_0 = 7800 \text{ kg/m}^3, \quad d_0 = 0.01 \text{ m},$$

$$\mu_1 = 7.69 \times 10^3 \text{ MPa}, \quad \rho_1 = 7800 \text{ kg/m}^3, \quad d_1 = 0.03 \text{ m}, \tag{19}$$

for the unit interface of Fig. 2a. Fig. 4b is given for structural interfaces with μ_0 , ρ_0 and d_0 given in Eq. (19) for the continuous phase and

$$m = 234 \text{ kg/m}^2, \quad \gamma = 5130 \times 10^3 \text{ MPa/m}, \tag{20}$$

for the structural interface, corresponding to inclined bars of Fig. 1 with

$$\eta = 0.2 \text{ rad}, \quad E = 24.2 \times 10^3 \text{ MPa}, \quad A = 0.1 \text{ m}^2/\text{m}. \tag{21}$$

It is shown that the structural interface in Fig. 4b has unique properties as a result of the ‘mix’ between continuous and discrete nature of the two layers composing the unit cell. It can transmit selected ranges of frequencies without an upper

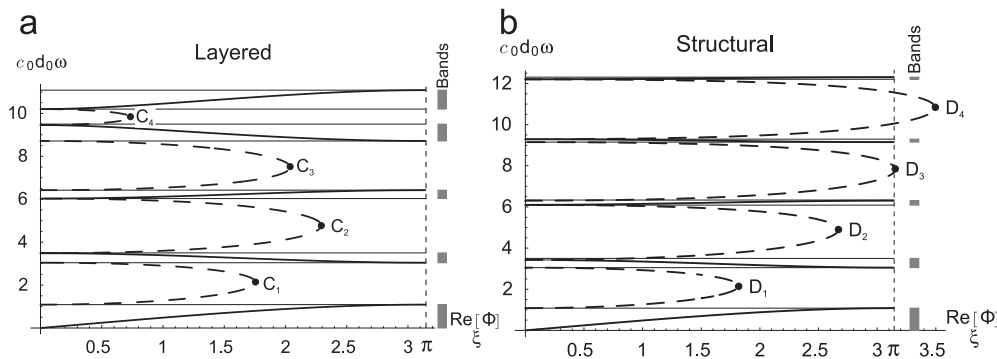


Fig. 4. Dispersion curves and decay exponent for thick interfaces (Eqs. (14), (15) and (18)). For propagating waves solid lines indicate the normalized angular frequency $c_0 d_0 \omega$ (rad) as a function of the Bloch parameter ϕ (rad). For non-propagating waves, dashed lines describe $c_0 d_0 \omega$ (rad) versus the decay exponent ξ (rad). (a) Layered interface (Eq. (19)). (b) Structural interface (Eqs. (19), (20) and (21)).

Table 1

Maximum decay exponents ξ and corresponding normalized frequency $c_0 d_0 \omega$ for the attenuation curves of Fig. 4, referred to layered (C_j) and structural (D_j) interfaces.

	C_1	C_2	C_3	C_4	D_1	D_2	D_3	D_4
ξ	1.76	2.29	2.04	0.74	1.82	2.67	3.15	3.49
$c_0 d_0 \omega$	2.13	4.78	7.49	9.82	2.16	4.89	7.83	10.83

limit. As a consequence of the introduction of the inertial truss structure, at increasing frequency ω the dispersion diagram presents narrower and narrower optical pass bands characterized by low group velocity, where the central frequency of such branches is determined by the continuous layers, as can be easily checked from the dispersion relation (15).

The comparative analysis of the dispersion diagrams in Figs. 4a and b suggests that for the low frequencies, covering the first three pass bands, the dispersion curves for layered and structural interfaces agree well with each other. On the other hand, a visible difference exists for evanescent waves, even at low frequencies, which is reflected in the values of the localization exponent ξ plotted dashed and correspondingly by the coordinates of the points C_j, D_j ($j=1, \dots, 4$), characterizing the ‘depth’ of the band gaps.

The decay exponent ξ displays a maximum at a frequency within each stop band; these maxima, labeled C_j and D_j in Fig. 4 and reported in Table 1, correspond to the frequencies providing the maximum wave attenuation. For the structural interface the maximum decay exponents increase at increasing frequency ω , while this is not true for the layered elastic interfaces.

Regarding the continuous layered interface, computations summarized in Fig. 4 show that, with the choice

$$\rho_1 d_1 = m \quad \text{and} \quad 2 \frac{\mu_1}{d_1} = \gamma, \tag{22}$$

the two types of interfaces may display very similar dispersion properties at low frequencies.

On the contrary, for higher frequencies the structure of pass bands in Figs. 4a and b remains different. In particular, the pass bands for the structural interface do not show periodicity (in the frequency spectrum of ω), as one would expect in the case of the layered medium.

3.3. Reflection and transmission properties for structural interfaces

Let us consider a structural interface, composed of a finite number of continuous-elastic and structural layers, embedded in an infinite elastic medium, with constants ρ_α and μ_α on the left of the layer and ρ_β and μ_β on the right. The incident and reflected waves on the left of the interface admit the representation

$$u(x) = A_I \exp(ik_\alpha x) + A_R \exp(-ik_\alpha x), \tag{23}$$

where A_I and A_R are the incident and reflection amplitudes, while the transmitted wave on the right of the interface is given by

$$u(x) = \sqrt{\frac{\mu_\alpha}{\mu_\beta}} A_T \exp(ik_\beta x), \tag{24}$$

with A_T denoting the transmission amplitude.

The following system can be written upon the introduction of the appropriate transfer matrix characterizing the structured slab (see Section 3.1)

$$\sqrt{\frac{\mu_\alpha}{\mu_\beta}} \begin{bmatrix} A_T e^{ik_\beta x_1} \\ iQ_\beta A_T e^{ik_\beta x_1} \end{bmatrix} = [\mathbf{M}] \begin{bmatrix} A_I e^{ik_\alpha x_0} + A_R e^{-ik_\alpha x_0} \\ iQ_\alpha (A_I e^{ik_\alpha x_0} - A_R e^{-ik_\alpha x_0}) \end{bmatrix}, \tag{25}$$

(where $Q_\alpha = \mu_\alpha k_\alpha$ and $Q_\beta = \mu_\beta k_\beta$), which can be solved for the amplitudes A_R and A_T of the reflected and transmitted waves in the form

$$\begin{aligned} \bar{A}_R &= \frac{Q_\alpha Q_\beta m_{12} + m_{21} + i(Q_\alpha m_{22} - Q_\beta m_{11})}{Q_\alpha Q_\beta m_{12} - m_{21} + i(Q_\alpha m_{22} + Q_\beta m_{11})} e^{2ik_\alpha x_0}, \\ \bar{A}_T &= \sqrt{\frac{\mu_\beta}{\mu_\alpha}} \frac{2iQ_\alpha}{Q_\alpha Q_\beta m_{12} - m_{21} + i(Q_\alpha m_{22} + Q_\beta m_{11})} e^{i(k_\alpha x_0 - k_\beta x_1)}, \end{aligned} \tag{26}$$

where we have introduced the normalization $\bar{A}_R = A_R/A_I$, $\bar{A}_T = A_T/A_I$.

The normalized reflected R and transmitted $T=1-R$ energies are given by

$$R = |\bar{A}_R|^2 = \frac{(Q_\alpha Q_\beta m_{12} + m_{21})^2 + (Q_\alpha m_{22} - Q_\beta m_{11})^2}{(Q_\alpha Q_\beta m_{12} - m_{21})^2 + (Q_\alpha m_{22} + Q_\beta m_{11})^2},$$

$$T = |\bar{A}_T|^2 \frac{Q_\beta}{Q_\alpha} = \frac{4Q_\alpha Q_\beta}{(Q_\alpha Q_\beta m_{12} - m_{21})^2 + (Q_\alpha m_{22} + Q_\beta m_{11})^2}, \quad (27)$$

so that we have total transmission for $R=0$ ($T=1$) and total reflection for $R=1$ ($T=0$).

In the case of a structured slab made up of a p -repetition of the unit cells as shown in Fig. 2, the normalized reflection and transmission amplitudes are obtained using the transfer matrix given by Eq. (10) or by Eq. (11)

$$\bar{A}_R = \frac{Q_\alpha Q_\beta m_{12} + m_{21} + i(Q_\alpha(m_{22} - \sigma_p) - Q_\beta(m_{11} - \sigma_p))}{Q_\alpha Q_\beta m_{12} - m_{21} + i(Q_\alpha(m_{22} - \sigma_p) + Q_\beta(m_{11} - \sigma_p))} e^{2ik_x x_0},$$

$$\bar{A}_T = \sqrt{\frac{\mu_\beta}{\mu_\alpha}} \frac{2iQ_\alpha S_p^{-1}(x) e^{i(k_\alpha x_0 - k_\beta x_p)}}{Q_\alpha Q_\beta m_{12} - m_{21} + i(Q_\alpha(m_{22} - \sigma_p) + Q_\beta(m_{11} - \sigma_p))}, \quad (28)$$

with $x_p - x_0 = pd$. The parameter $\sigma_p(x) = S_{p-1}(x)/S_{p-2}(x)$ in Eq. (28) takes into account that the slab is made up of p unit cells. The reflected and transmitted energies are

$$R = \frac{(Q_\alpha Q_\beta m_{12} + m_{21})^2 + (Q_\alpha(m_{22} - \sigma_p) - Q_\beta(m_{11} - \sigma_p))^2}{(Q_\alpha Q_\beta m_{12} - m_{21})^2 + (Q_\alpha(m_{22} - \sigma_p) + Q_\beta(m_{11} - \sigma_p))^2},$$

$$T = \frac{4Q_\alpha Q_\beta S_p^{-2}(x)}{(Q_\alpha Q_\beta m_{12} - m_{21})^2 + (Q_\alpha(m_{22} - \sigma_p) + Q_\beta(m_{11} - \sigma_p))^2}. \quad (29)$$

Finally, we note that, in the absence of the layer ($\mathbf{M}=\mathbf{I}$ and $d=0$), Eqs. (26) provide the reflection and transmission amplitudes at a perfect interface separating two infinite media of elastic contrast μ_α/μ_β , namely,

$$\bar{A}_R = \frac{Q_\alpha - Q_\beta}{Q_\alpha + Q_\beta} e^{2ik_x x_0}, \quad \bar{A}_T = \sqrt{\frac{\mu_\beta}{\mu_\alpha}} \frac{2Q_\alpha}{Q_\alpha + Q_\beta} e^{i(k_\alpha - k_\beta)x_0}, \quad (30)$$

and the reflected and transmitted energies, given by Eqs. (27) simplify now to

$$R = \frac{(Q_\alpha - Q_\beta)^2}{(Q_\alpha + Q_\beta)^2}, \quad T = \frac{4Q_\alpha Q_\beta}{(Q_\alpha + Q_\beta)^2}. \quad (31)$$

3.3.1. Structural interfaces joining two elastic half spaces

We consider the elastic system described in the upper part of Fig. 5b where two different elastic half spaces (labeled α and β as in the previous section) are joined by a structural interface made up of two springs of stiffness γ and a concentrated mass m .

In such a case, the reflected energy is

$$R = \frac{(Q_\alpha - Q_\beta)^2 (\gamma - m\omega^2)^2 \gamma^2 + [m\omega^2 \gamma^2 - Q_\alpha Q_\beta (2\gamma - m\omega^2)]^2}{(Q_\alpha + Q_\beta)^2 (\gamma - m\omega^2)^2 \gamma^2 + [m\omega^2 \gamma^2 + Q_\alpha Q_\beta (2\gamma - m\omega^2)]^2}. \quad (32)$$

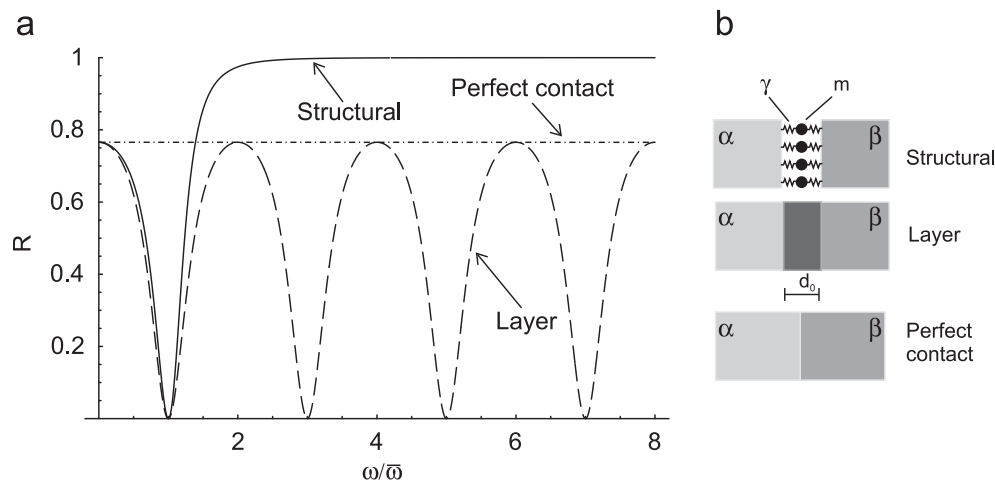


Fig. 5. Reflected energy R as a function of the normalized frequency $\omega/\bar{\omega}$ for: (i) a structural interface and (ii) a one-layer interface connecting semi-infinite media α and β , with $\mu_\alpha = 10$ MPa, $\rho_\alpha = 1000$ kg/m³, and $\mu_\beta = 450$ MPa, $\rho_\beta = 5000$ kg/m³. Results are also compared to the situation in which the two half spaces are jointed with a perfect contact condition (namely, without any structural or layered interface). These three situations are sketched in part (b): structural interface with $c/\bar{\omega} = m\bar{\omega} = 0.287$ MPa s (solid line), layered interface with $\mu_0 = 50$ MPa, $\rho_0 = 3000$ kg/m³, $d_0\bar{\omega} = 202.8$ m/s (dashed line) and perfect contact (dashed-dotted line).

Note that, for given properties of the elastic half spaces $(\mu_\alpha, \mu_\beta, \rho_\alpha, \rho_\beta)$ and prescribed frequency $\bar{\omega}$, we can select the stiffness of the spring and the mass of the system as

$$\gamma = \bar{\omega} \sqrt[4]{\mu_\alpha \mu_\beta \rho_\alpha \rho_\beta}, \quad m = \frac{\sqrt[4]{\mu_\alpha \mu_\beta \rho_\alpha \rho_\beta}}{\bar{\omega}}, \quad (33)$$

(corresponding to the internal resonance mode of the structural interface), so that we obtain a *total transmission condition*, a property which *cannot* be achieved in the case of a non-inertial interface. In fact, for $m=0$ the reflected energy becomes

$$R = \frac{\gamma^2(Q_\alpha - Q_\beta)^2 + 4Q_\alpha^2 Q_\beta^2}{\gamma^2(Q_\alpha + Q_\beta)^2 + 4Q_\alpha^2 Q_\beta^2}, \quad (34)$$

(reducing to $R = 1/(1 + \gamma^2)$ if $Q_\alpha = Q_\beta$), which is a monotonically decreasing function of the stiffness γ ranging from

$$R = \frac{(Q_\alpha - Q_\beta)^2}{(Q_\alpha + Q_\beta)^2}, \quad (35)$$

when $\gamma \rightarrow \infty$, as in Eq. (31a), to $R=1$ when $\gamma=0$ (in which case the two half spaces are disconnected). This simple result underlines the role of the inertial effects in the interface for the reduction of the amount of energy reflection.

In the case of an interface made up of an elastic layer, the reflected energy can be calculated as

$$R = \frac{Q_0^2(Q_\alpha - Q_\beta)^2 \cos^2(c_0 d_0 \omega) + (Q_0^2 - Q_\alpha Q_\beta)^2 \sin^2(c_0 d_0 \omega)}{Q_0^2(Q_\alpha + Q_\beta)^2 \cos^2(c_0 d_0 \omega) + (Q_0^2 + Q_\alpha Q_\beta)^2 \sin^2(c_0 d_0 \omega)}, \quad (36)$$

which for given $\mu_\alpha, \mu_\beta, \rho_\alpha, \rho_\beta$, and frequency $\bar{\omega}$ can be zero if and only if

$$\mu_0 \rho_0 = \sqrt{\mu_\alpha \mu_\beta \rho_\alpha \rho_\beta}, \quad d_0 = \frac{1}{\bar{\omega}} \left(\frac{\pi}{2} + n\pi \right) \sqrt{\frac{\mu_0}{\rho_0}}, \quad (37)$$

for every $n \in \mathbb{N}^+ \setminus \{0\}$. Therefore, a total transmission condition can be achieved through both the structural interface and the layer interface. However, the differences between the two systems are substantial. With reference to Fig. 5 (obtained for $\mu_\alpha = 10$ MPa, $\rho_\alpha = 1000$ kg/m³, and $\mu_\beta = 450$ MPa, $\rho_\beta = 5000$ kg/m³), we see that, even for high contrast between the elastic media, the structural interface allows us to obtain a sharp filter, leaving full transmission for the frequency $\omega = \bar{\omega}$ and practically truncating all higher frequencies. The interface obtained with the elastic layer realizes the total transmission condition for infinite countable frequencies $\omega/\bar{\omega} = 1 + 2n$ ($n \in \mathbb{N}^+ \setminus \{0\}$), and practically does not truncate higher frequencies (R is always inferior than 0.77). This provides us with an example of a dynamical effect which can be achieved *only* with a structural interface.

3.3.2. Results for layered and structural interfaces

We focus now the attention on the transmission properties of layered and structural interfaces, structures which may find applications in the design of delay lines for wave guide systems for elastic waves. We report in Fig. 6 the normalized reflected energy $R \in [0, 1]$ as a function of the normalized frequency $c_0 d_0 \omega$ for finite slabs composed of $p=4$ unit interfaces, the same as those considered in Fig. 4. The finite thickness interface is interposed between elastic media labeled α and β , with: $\mu_\alpha = 200$ MPa, $\rho_\alpha = 5000$ kg/m³, $\mu_\beta = 100 \times 10^3$ MPa, $\rho_\beta = 16\,000$ kg/m³.

It is clearly shown that the presence of a finite number of unit cells creating the interfaces generates oscillations in the reflected energy, so that it becomes possible to select finite ranges of frequency in which the reflection is very small or even approaches zero, by optimally designing the unit cell. This is a remarkable result, since we have seen that in the case of two elastic solids in perfect contact [$p=0$, see Eq. (31)], the reflected energy is $R=90.5\%$ and the reflected energy is even higher in the case of infinitely many (periodic, $p \rightarrow \infty$) unit cells, as shown in Felbacq et al. (1998) (who proved that the reflected energy tends to the superior envelope of the R -curves, when $p \rightarrow \infty$). Therefore, the fact that the interface has a finite thickness allows to dramatically change the transmission properties, as we have already noticed in the simpler case of one structural interface.

As in Section 3.2.1, we can observe the agreement in the transmission properties of the structural interface and its continuous layered counterpart (see Fig. 6b). However, for higher frequency pass bands, shown in Fig. 6a, the oscillations in the reflected energy are visibly different for the cases of structural and layered interfaces. This distinction is shown in greater detail in Fig. 6c, which suggests that the slow waves can be transmitted through a structured interface, but the frequencies of such transmission will be different for the structural interface and its homogenized continuous layered counterpart. Needless to say, the oscillations within a pass band region are linked to the resonance frequencies of the finite stack, and the number of oscillations increases with the increase of the number of elementary cells placed within the stack.

It follows from Figs. 4 and 6 that the oscillations in the reflected energy R correspond to the optical and acoustic branches in the dispersion diagrams, whereas in the stop bands $R \rightarrow 1$. If we concentrate our attention on the optical branches, we can select a frequency range in which the wave propagates with low group velocity, but still without reflecting a substantial amount of energy. This is an important property that can be achieved also with a small number of unit cells and can be used to build delay line devices for elastic waves.

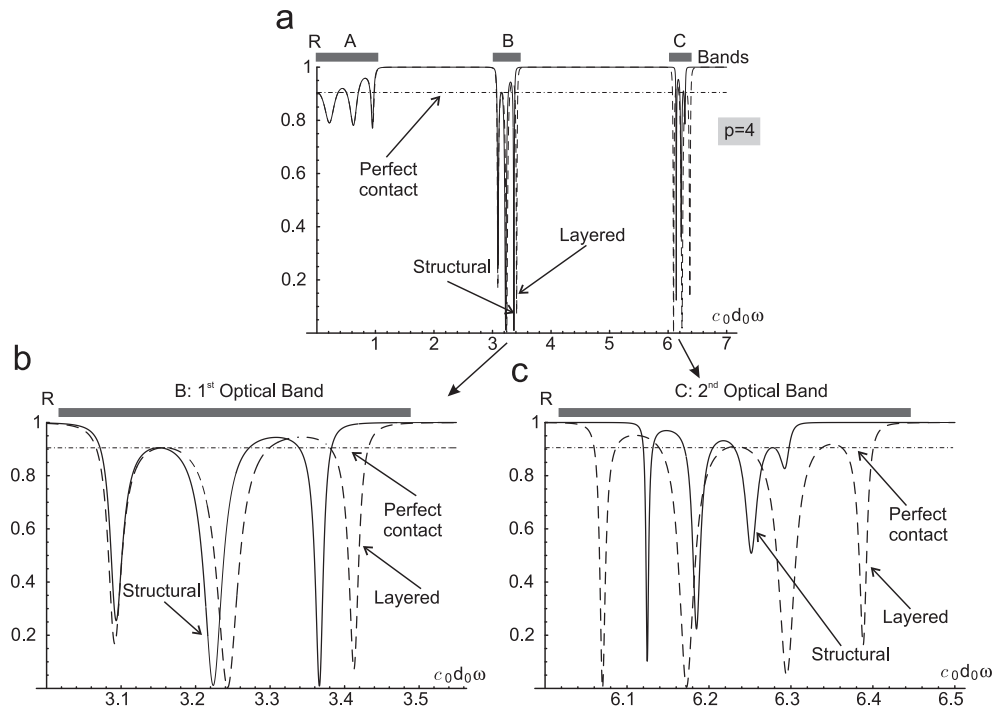


Fig. 6. Reflected energy R as a function of the normalized frequency $c_0 d_0 \omega$ for an interface composed of $p=4$ unit cells and connecting two elastic media α and β , with $\mu_\alpha = 200$ MPa, $\rho_\alpha = 5000$ kg/m³, and $\mu_\beta = 100 \times 10^3$ MPa, $\rho_\beta = 16000$ kg/m³. Results are given for structural interface (solid line) and layered interface (dashed line) and compared to the situation in which the two half spaces are perfectly connected (dashed-dotted line). The unit cells are the same as in Fig. 4. The diagrams (b) and (c) show in detail the reflected energy within the frequency ranges B and C. The figure shows that with optimally designed thick interfaces reflected energy can be ‘tuned’ and that the full transmission condition can be approached.

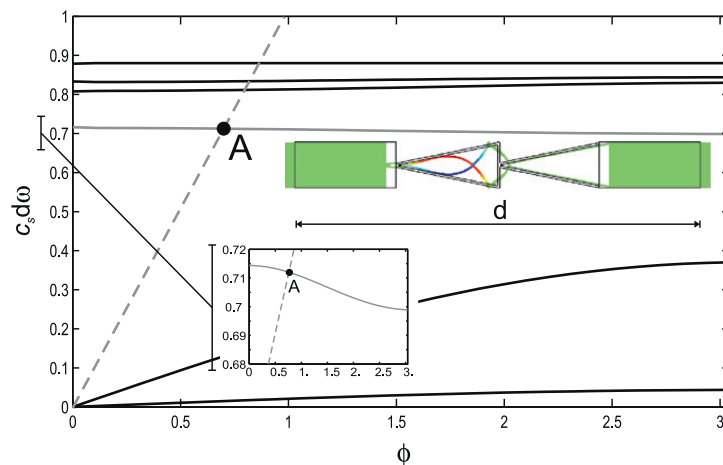


Fig. 7. Dispersion curves for a structural interface. The results correspond to fused silica for both the structure and the ambient media. The normalized elastic parameters are: Lamé constants ratio $\lambda/\mu = 2.3$, phase velocity $v_s = \sqrt{\mu/\rho} = 1$ m/s. Point A: intersection between the first optical branch (continuous grey line) and dispersion curve for shear waves propagating in homogeneous isotropic elastic space (dashed grey line). The localized eigenmode at point A is reported in color in the insert.

4. Negative refraction. Focussing of elastic waves by a flat lens

A structural interface can be adopted to design a flat device exhibiting a negative refraction within a suitably chosen interval of frequencies. For the purpose of illustration, we consider the structural interface introduced in Fig. 1. The elementary cell is shown in the insert of Fig. 7 and in Fig. 8, with the structure being periodic in the z direction.

We use a homogeneous isotropic elastic medium on the right and on the left of the discrete interface. The material parameters for the structure and the ambient medium are the same and correspond to normalized moduli for fused silica. We consider the ratio $\lambda/\mu = 2.3$ between the Lamé constants and a density ρ tailored to give a shear velocity in the homogeneous media $v_s = (c_s)^{-1} = \sqrt{\mu/\rho} = 1$ m/s.

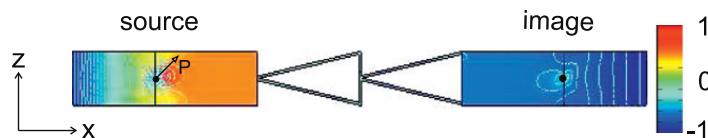


Fig. 8. Focussing effect for a point source (inclined at 45° and sketched black) at normalized frequency $c_s d\omega = 0.71$ rad, corresponding to the point A in Fig. 7.

The choice of the appropriate range of frequencies for which negative refraction and focussing is observed is clarified as follows. For the periodic discrete structure consisting of infinite doubly periodic arrays of elementary cells, the dispersion diagram in Fig. 7 shows the normalized frequency $c_s d\omega$ as a function of the Bloch parameter ϕ . The slope of the dashed grey ray emanating from the origin, given by

$$\frac{c_s d\omega}{\phi} = \frac{c_s \omega}{k} = 1 \quad (38)$$

is chosen to correspond to a shear wave propagating in the ambient homogeneous elastic medium, which is non-dispersive. The frequency $c_s d\omega = 0.71$ rad is then chosen to correspond to the intersection point A between this ray and the first 'optical mode' on the dispersion diagram.

Then, a transmission problem is considered for the interface and a point source, placed sufficiently close to the interface boundary (and indicated with an arrow in Fig. 8). The eigenmode shown in the insert of Fig. 7 corresponds to the time harmonic displacement field at the point A of intersection of the shear wave ray and the 'optical dispersion curve'; we note that the group velocity at this particular point is negative. The pulsating force is applied inclined at 45° . The result shown in Fig. 8 displays the mirror image of the point source on the right side of the interface. Although some changes occur when the orientation of the point force is altered, the current computation delivers a good illustrative example of a structural interface, where slow waves can be used to model negative refraction and focussing of elastic waves.

The example demonstrates that a structured interface of appropriate type is applicable for modeling metamaterials of desired filtering properties. In particular, the interface can be designed to transmit slow waves of certain frequencies and to exhibit negative refraction, leading to a focussing effect.

5. Conclusions

Numerical analyses under the Bloch–Floquet condition and analytical results obtained on simple homogenized structural models for the interface (via the transfer matrix technique) substantiate the conclusion that elastodynamics of structural interfaces opens new possibilities in the design of filtering devices for elastic waves. It has been shown that certain filtering properties can be achieved only by employing structural, instead of continuous, interfaces. Finally, a first example has been given in which a pulsating point force located at the left of a structural interface displays a symmetric image on the right of it, thus behaving as a flat lens for elastic waves via negative refraction. This result may prelude the possibility of obtaining high-resolution focussing properties for elastodynamic waves employing structural interfaces, a finding which could be used for the design of apparatuses for various applications, for instance, medical.

Acknowledgments

Part of this research was performed while two of the authors were visiting faculty at the Department of Mathematical Sciences, University of Liverpool (D.B. and M.B.) and at the Institute of Mathematics and Physics of the University of Aberystwyth (D.B.). M.B. visited Liverpool University under the EPSRC-GB Grant no. EP/F027125/1. D.B. also gratefully acknowledges financial support from PRIN Grant no. 2007YZ3B24 'Multi-scale Problems with Complex Interactions in Structural Engineering' financed by Italian Ministry of University and Research.

References

- Bertoldi, K., Bigoni, D., Drugan, J.W., 2007a. Structural interfaces in linear elasticity. Part I: nonlocality and gradient approximations. *J. Mech. Phys. Solids* 55 (1), 1–34.
- Bertoldi, K., Bigoni, D., Drugan, J.W., 2007b. Structural interfaces in linear elasticity. Part II: effective properties and neutrality. *J. Mech. Phys. Solids* 55 (1), 35–63.
- Bertoldi, K., Bigoni, D., Drugan, J.W., 2007c. A discrete-fibers model for bridged cracks and reinforced elliptical voids. *J. Mech. Phys. Solids* 55 (5), 1016–1035.
- Bigoni, D., Gei, M., Movchan, A.B., 2008. Dynamics of a prestressed stiff layer on an elastic half space: filtering and band gap characteristics of periodic structural models derived from longwave asymptotics. *J. Mech. Phys. Solids* 56 (7), 2494–2520.
- Bigoni, D., Movchan, A.B., 2002. Statics and dynamics of structural interfaces in elasticity. *Int. J. Solids Struct.* 39 (19), 4843–4865.
- Brun, M., Guenneau, S., Movchan, A.B., 2009. Achieving control of in-plane elastic waves. *Appl. Phys. Lett.* 94 (6), 061903.
- Ding, Y., Liu, Z., Qiu, C., Shi, J., 2007. Metamaterial with simultaneously negative bulk modulus and mass density. *Phys. Rev. Lett.* 99 (9), 093904.
- Farhat, M., Guenneau, S., Enoch, S., Movchan, A.B., 2008. Broadband cylindrical acoustic cloak for linear surface waves in a fluid. *Phys. Rev. Lett.* 101 (13), 134501.

- Felbacq, D., Guizal, B., Zolla, F., 1998. Limit analysis of the diffraction of a plane wave by a one-dimensional periodic medium. *J. Math. Phys.* 39 (9), 4604–4607.
- Gei, M., Movchan, A.B., Bigoni, D., 2009. Band-gap shift and defect-induced annihilation in prestressed elastic structures. *J. Appl. Phys.* 105 (6), 063507.
- Guenneau, S., Movchan, A.B., Petrusson, G., Ramakrishna, S.A., 2007. Acoustic metamaterials for sound focussing and confinement. *New J. Phys.* 9, 399.
- Guenneau, S., Movchan, A.B., Movchan, N.V., Trebicki, J., 2008. Acoustic stop bands in almost-periodic and weakly randomized stratified media: perturbation analysis. *Acta Mech. Sin.* 24 (5), 549–556.
- Lekner, J., 1994. Light in periodically stratified media. *J. Opt. Soc. Am. A* 11 (11), 2892–2899.
- Leonhardt, U., Philbin, T.G., 2006. General relativity in electrical engineering. *New J. Phys.* 8, 247.
- Martinsson, P.G., Movchan, A.B., 2003. Vibrations of lattice structures and phononic band gaps. *Q. J. Mech. Appl. Math.* 56, 45–64.
- Milton, G.W., Willis, J.R., 2007. On modifications of Newton's second law and linear continuum elastodynamics. *Proc. R. Soc. London A* 463 (2079), 855–880.
- Milton, G.W., Nicorovici, N.A.P., 2006. On the cloaking effects associated with anomalous localized resonance. *Proc. R. Soc. London A* 462 (2074), 3027–3059.
- Milton, G.W., Nicorovici, N.A.P., McPhedran, R.C., Cherednichenko, K., Jacob, Z., 2008. Solutions in folded geometries, and associated cloaking due to anomalous resonance. *New J. Phys.* 10, 115021.
- Movchan, A.B., Guenneau, S., 2004. Split-ring resonators and localized modes. *Phys. Rev. B* 70 (12), 125116.
- Movchan, A.B., Slepyan, L.I., 2007. Band gap Green's functions and localized oscillations. *Proc. R. Soc. London A* 463 (2086), 2709–2727.
- Parnell, W.J., 2007. Effective wave propagation in a prestressed nonlinear elastic composite bar. *IMA J. Appl. Math.* 72 (2), 223–244.
- Pendry, J.B., 2000. Negative refraction makes a perfect lens. *Phys. Rev. Lett.* 85 (18), 3966–3969.
- Pendry, J.B., Holden, A.J., Robbins, D.J., Stewart, W.J., 1999. Magnetism from conductors and enhanced nonlinear phenomena. *IEEE Trans. Microwave Theory Tech.* 47 (11), 2075–2084.
- Pendry, J.B., Schurig, D., Smith, D.R., 2006. Controlling electromagnetic fields. *Science* 312, 1780.
- Platts, S.B., Movchan, N.V., 2004. Phononic band gap properties of doubly periodic arrays of coated inclusions. In: Bergman, D.J., Inan, E. (Eds.), *Continuum Models and Discrete Systems*, NATO Science Series II: Mathematics, Physics and Chemistry, vol. 158. Kluwer Academic Publishers, pp. 287–294.
- Robbie, K., Brett, M.J., Lakhtakia, A., 1996. Chiral sculptured thin films. *Nature* 384 (6610), 616.
- Robbie, K., Broer, D.J., Brett, M.J., 1999. Chiral nematic order in liquid crystals imposed by an engineered inorganic nanostructure. *Nature* 399 (6738), 764–766.
- Smith, D.R., Kroll, N., 2000. Negative refractive index in left-handed materials. *Phys. Rev. Lett.* 85 (14), 2933–2936.
- Sukhovich, A., Jing, L., Page, J.H., 2008. Negative refraction and focussing of ultrasound in two-dimensional phononic crystals. *Phys. Rev. B* 77 (1), 014301.
- Sumigawa, T., Hirakata, H., Takemura, M., Matsumoto, S., Suzuki, M., Kitamura, T., 2008. Disappearance of stress singularity at interface edge due to nanostructured thin film. *Eng. Fract. Mech.* 75 (10), 3073–3083.
- Tang, T., Hui, C.-Y., Glassmaker, N.J., 2005. Can a fibrillar interface be stronger and tougher than a non-fibrillar one? *J. R. Soc. Interface* 2 (5), 505–516.
- Veselago, V.G., 1968. Electrodynamics of substances with simultaneously negative value of ϵ and μ . *Sov. Phys. Uspekhi* 10, 509–514.
- Zhang, S., Yin, L., Fang, N., 2009. Focussing ultrasound with an acoustic metamaterial network. *Phys. Rev. Lett.* 102 (19), 194301.